Yang, R., et al., 2023, Stable tungsten isotopic composition of seawater over the past 80 million years: Geology, https://doi.org/10.1130/G51208.1

Supplemental Material

Figures S1–S4.

Supplementary Text and Figure Captions.

Supplementary materials for

Stable tungsten isotopic composition of seawater over the past 80 million years

Ruiyu Yang[1,2,3], Daniel Stubbs[4], Tim Elliott[4], Tao Li[5], Tianyu Chen[1], Adina Paytan[6], David B. Kemp[7], Hongfei Ling[1], Jun Chen[1], James R. Hein[8], Christopher D. Coath[4], Gaojun Li[1]*

[1]*Department of Earth and Planetary Sciences, Nanjing University, Nanjing 210023, China.*

[2]*Institute for Geology and Mineralogy, University of Cologne, Cologne 50674, Germany*

[3]*GEOMAR Helmholtz Centre for Ocean Research, Kiel 24148, Germany*

[4]*School of Earth Sciences, University of Bristol, Bristol BS8 1RJ, UK.*

[5]*State Key Laboratory of Palaeobiology and Stratigraphy, Nanjing Institute of Geology and Palaeontology, Nanjing 210008, China*

[6]*Institute of Marine Sciences, University of California, Santa Cruz, CA 95064, USA.*

[7]*State Key Laboratory of Biogeology and Hubei Key Laboratory of Critical Zone Evolution, School of Earth Sciences, China University of Geosciences, Wuhan 430074, China.*

[8]*U.S. Geological Survey (Retired), Santa Cruz, CA 95060, USA.*

Supplementary text

Sample pretreatment

Subsamples of 3-4 mg each were taken from the CJ01, MDD53 and Yaloc crusts using a dental drill with a diamond abrasive coated tip. The surface of the crust and the drill pits were carefully cleaned using Kimtech® wipers damped with Milli-Q water between each drilling to avoid cross contamination. The distance between sub-samples was 2.5-5.0 mm perpendicular to the growth axis for crusts CJ01 and MDD53. The sub-samples of the Yaloc crust were taken from exactly the same locations used for ^{10}Be dating (van de Flierdt et al., 2004) with an average distance of 6.0 mm. Subsamples of Fe-Mn crusts were digested in concentrated HCl overnight in Savillex™ Teflon beakers on a hotplate at 120 °C. After complete dissolution, samples were dried and converted into nitrate form by addition of 4 ml concentrated HNO_3, and subsequently evaporated to dryness. The digested solution was optimally spiked according to the concentration of tungsten (W) measured by the Quadrupole ICP-MS. The spiked samples were equilibrated overnight, dried, and re-dissolved with 1 M HCl – 1 M HF for ion exchange chromatography.

Column separation of W and isotopic measurement

The BioRad AG 1 × 8 anionic resin (100-200 mesh, 4 ml) was used for column separation of W. The detailed column procedure is outlined in Yang et al. (2022) and Stubbs et al. (2022). The overall procedural blank is 0.1-0.2 ng, contributing < 1‰ to the analyzed W. Tungsten isotope ratios were measured using a Neptune Plus multi-collector inductively coupled plasma mass spectrometer (MC-ICPMS) at MOE Key Laboratory of Surficial Geochemistry (KLSG), Nanjing University. Samples were introduced to the plasma using a 50 μl/min PFA nebulizer connected to Cetac Aridus desolvating system. Nickel Jet 'J' sample cone and nickel 'H' skimmer cones were used. All five W isotopes (^{180}W, ^{182}W, ^{183}W, ^{184}W, and ^{186}W) were measured simultaneously on faraday cups connected to 10^{11} Ω resistors. Interferences from Os were monitored by measuring ^{188}Os, but were never above instrumental baseline and no interference corrections were necessary. Typical sensitivity (sum of all individual W ion beams) was ~200 pA for a 40 ng g^{-1} solution. Gain calibration was done before each session. Samples were run in 0.4 M HNO_3 - 0.4 M HF. An uptake of approximately 70 s allowed the beam to stabilize. Each measurement was 40 cycles of 8.4 seconds integration time, followed by 270 seconds washing, and then an on peak measurement of the blank solution was subtracted from sample intensities before further calculations. All samples were measured at least three times. Detailed measurement parameters are presented by Yang et al. (2022).

The sample $\delta^{186/184}W$ was calculated using the natural fractionation factor α following the method of (Rudge et al., 2009). Stable W isotope ratios are reported relative to NIST SRM 3163, i.e., $\delta^{186/184}W_{sample} = [(^{186}W/^{184}W_{\ sample} - {}^{186}W/^{184}W_{\ NIST\ 3163}) / (^{186}W/^{184}W_{\ NIST\ 3163})] \times 1000$. The value of $\delta^{186/184}W$ is reported as parts per thousand deviations (‰). Repeated analyses of Fe-Mn nodule standard NOD-P-1 through the entire chemical separation and measurement procedure indicate a reproducibility better than 0.04‰ (2 s.d., n = 17) (Yang et al., 2022).

Calculation of authigenic W fluxes and $\delta^{186/184}W$ compositions

Authigenic W (W_{auth}), excluding the lithogenic W fraction, is calculated from the W concentrations and the W/Th (or W/Al) ratios of the upper continental crust (Rudnick and Gao, 2014):

$$W_{auth} = W_{total} - (W/Al)_{UCC} \times Al_{total}$$

$$W_{auth} = W_{total} - (W/Th)_{UCC} \times Th_{total}$$

The authigenic fractions of all the sediments were corrected with W/Th, except for those obtained from IODP Site U1457, of which the Th concentration data was not available. For these sediments, we utilized W/Al instead (Table S2). The authigenic $\delta^{186/184}W$ ($\delta^{186/184}W_{auth}$) values were extrapolated from the $\delta^{186/184}W_{total}$ and the $\delta^{186/184}W_{UCC}$:

$$\delta^{186/184}W_{auth} = \frac{^{186}W/^{184}W_{\ total} - (1 - W_{auth}/W_{total}) \times \delta^{186/184}W_{UCC}}{W_{auth}/W_{total}}$$

The $\delta^{186/184}W_{UCC}$ is 0.01 ± 0.01‰ based on loess samples from Chinese Loess Plateau which incorporated a large area of continents and were homogenously mixed (Yang et al., 2022). The seawater $\delta^{186/184}W$ compositions ($\delta^{186/184}W_{sw}$) were calculated from the Fe-Mn crusts (smoothed average values for three Fe-Mn crusts in this study, Table S2) assuming a constant fractionation offset (0.58 ± 0.05‰) between seawater and the crusts. The $\Delta_{SW\text{-}sink}$ values are the $\delta^{186/184}W$ of simultaneous seawater subtracted by the respective authigenic $\delta^{186/184}W$ values ($\delta^{186/184}W_{auth}$, Table S2). Taking into account the error propagation of $\delta^{186/184}W$ values for Fe-Mn crusts (±0.04‰) and seawater estimation (±0.05‰), the ± 2 × external standard deviation for $\Delta_{SW\text{-}sink}$ can be estimated at ±0.06‰.

Th concentrations in Table S2 were determined via Quadrupole ICPMS (Agilent 7900) analyses in KLSG, Nanjing University. External reproducibility of reference standard BCR-2 and in-house standards data was less than ±5% (RSD).

Figure S1

Locations of the three ferromanganese (Fe-Mn) crust samples (yellow stars) and ODP/IODP sediment cores (red dots).

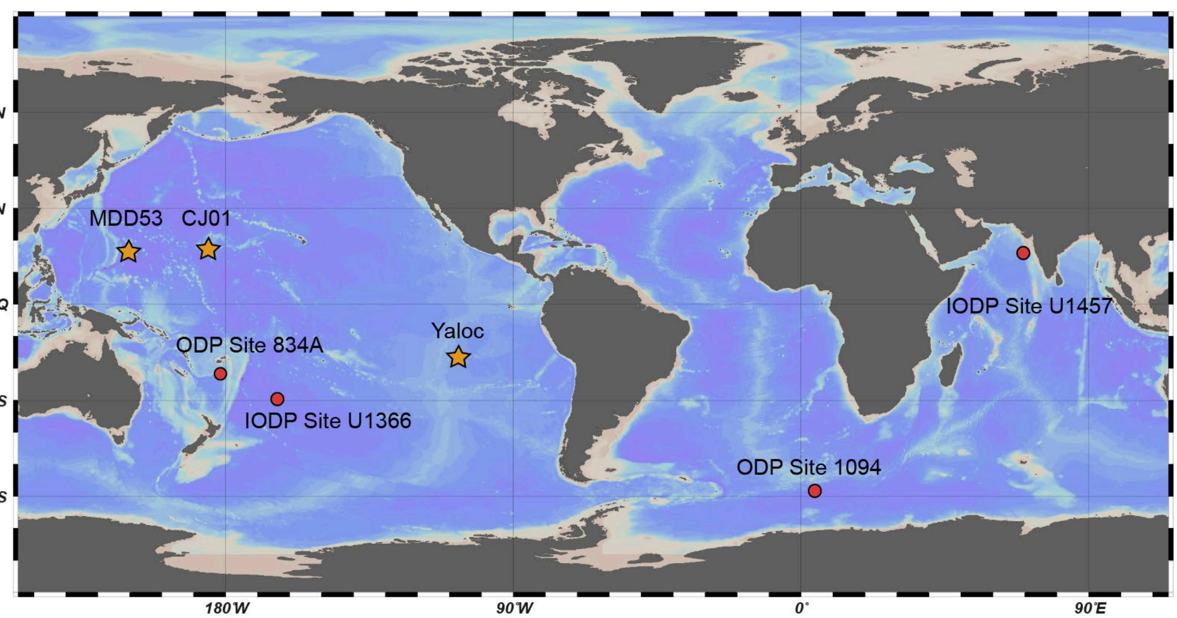

Figure S2

The $\delta^{186/184}W$ compositions of mixed hydrothermal-hydrogenetic crust (Yaloc). The sections of Fe-Mn crust that exhibit hydrothermal influences, as identified by Pb isotopes (van de Flierdt et al., 2004), are indicated by gray banded intervals. The error bars for $\delta^{186/184}W$ values represent the ±2 × external standard deviation (±0.04‰) based on long-time independent analyses on rock standards.

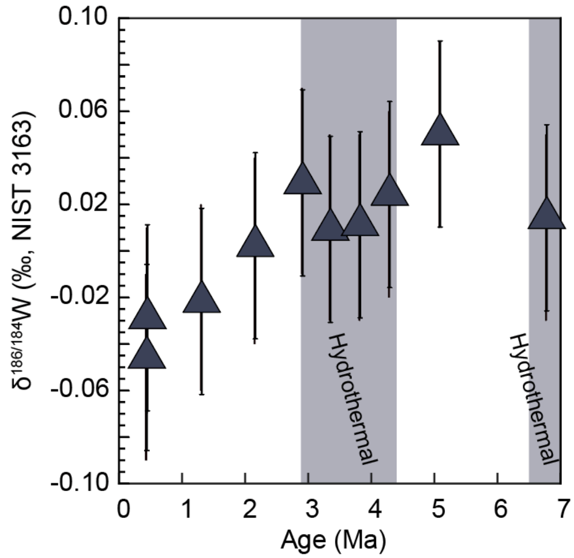

Figure S3

Cross plots of Mn/Fe ratios and $\delta^{186/184}W$ values of Fe-Mn crusts CJ01 (A) and MDD53 (B). The Mn and Fe concentration data are from Ling et al. (2005) and Liu et al. (2022, in Chinese). The error bars for $\delta^{186/184}W$ values represent the ±2 × external standard deviation (±0.04‰) based on long-time independent analyses on rock standards. The moving average values are represented by the fitted lines, and the shaded areas around them indicate the error range of ±2 × standard deviation.

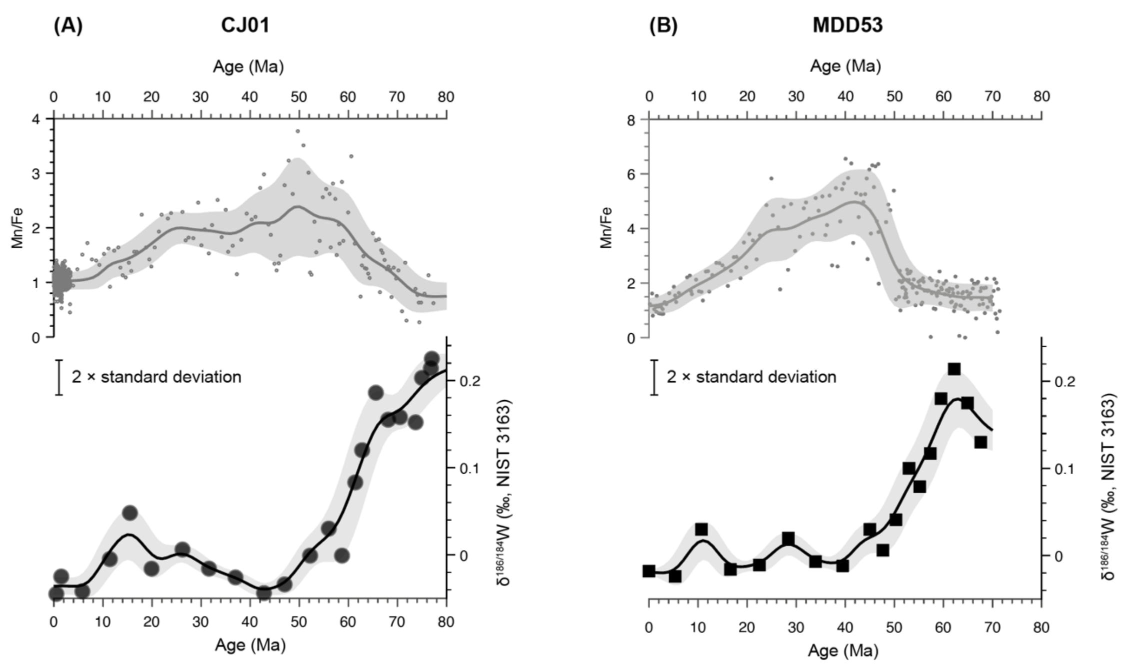

Figure S4

The $\delta^{186/184}W$ of Fe-Mn crusts MDD53 and CJ01 plotted against age. The error bars for $\delta^{186/184}W$ values represent the ±2 × external standard deviation (±0.04‰) based on long-time independent analyses on rock standards. The purple and green shaded areas are shown to represent the age errors of ±10%.

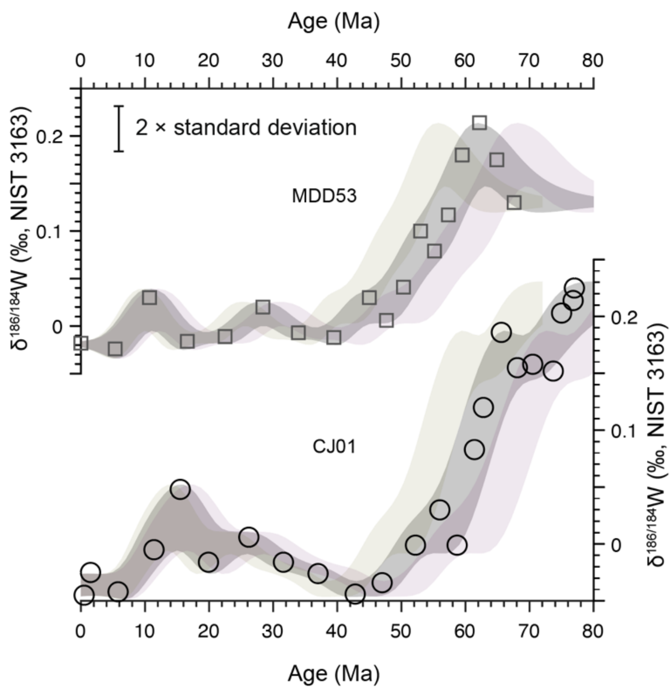

Table S1

The isotopic compositions and concentrations of W, along with the sampling depths and ages of Fe-Mn crust samples. The W concentrations were measured by the MC-ICP-MS and accurately calculated by isotope dilution using double spike. The ±2 × external standard deviation for $\delta^{186/184}W$ values is ±0.04‰ based on long-time independent analyses on rock standards.

Sample ID.	**Depth (mm)**	**Age (Ma)**	**$\delta^{186/184}W$ (‰)**	**[W] (μg g^{-1})**
MDD53-01	0.00	0.00	-0.02	42.01
MDD53-02	5.00	5.35	-0.02	42.11
MDD53-03	10.00	10.70	0.03	91.33
MDD53-04	15.00	16.60	-0.02	59.80
MDD53-05	20.00	22.50	-0.01	83.34
MDD53-06	25.00	28.40	0.02	75.24
MDD53-07	30.00	33.93	-0.01	70.61
MDD53-08	35.00	39.47	-0.01	111.88
MDD53-09	40.00	45.00	0.03	102.96
MDD53-10	45.00	47.67	0.01	58.19
MDD53-11	50.00	50.33	0.04	80.46
MDD53-12	55.00	53.00	0.10	134.12
MDD53-13	60.00	55.17	0.08	110.14
MDD53-14	65.00	57.33	0.12	81.50
MDD53-15	70.00	59.50	0.18	101.42
MDD53-16	75.00	62.20	0.21	49.32
MDD53-17	80.00	64.90	0.18	47.92
MDD53-18	85.00	67.60	0.13	54.82
CJ01-01	0.00	0.50	-0.05	50.52
CJ01-02	3.40	1.50	-0.03	59.53
CJ01-03	6.80	5.80	-0.04	50.17
CJ01-04	10.20	11.42	-0.01	51.96
CJ01-05	13.60	15.50	0.05	60.01
CJ01-06	17.00	19.85	-0.02	57.55
CJ01-07	20.40	26.19	0.01	61.65
CJ01-08	23.80	31.56	-0.02	61.98
CJ01-09	27.20	37.00	-0.03	72.68
CJ01-10	30.60	42.80	-0.04	75.60
CJ01-11	34.00	47.00	-0.03	53.98

CJ01-12	37.40	52.18	0.00	69.80
CJ01-13	40.80	56.00	0.03	58.28
CJ01-14	44.20	58.68	0.00	43.64
CJ01-15	47.60	61.40	0.08	48.45
CJ01-16	51.00	62.75	0.12	42.27
CJ01-17	54.40	65.60	0.19	45.05
CJ01-18	57.80	68.10	0.16	55.39
CJ01-19	61.20	70.50	0.16	50.81
CJ01-20	64.60	73.66	0.15	52.17
CJ01-21	68.00	75.00	0.20	48.02
CJ01-22	71.40	76.80	0.21	43.61
CJ01-23	74.80	77.00	0.23	44.40
Yaloc-01	0-1.0	0.43	-0.05	77.24
Yaloc-02	1.5-2.5	0.44	-0.03	79.86
Yaloc-03	5.5-6.5	1.30	-0.02	77.05
Yaloc-04	9.5-10.5	2.15	0.00	50.93
Yaloc-05	15-16	2.90	0.03	62.14
Yaloc-06	19.5-20.5	3.34	0.01	69.45
Yaloc-07	24-25	3.81	0.01	45.61
Yaloc-08	28.5-29.5	4.28	0.02	58.36
Yaloc-09	35-36	5.08	0.05	73.95
Yaloc-10	61-62	6.77	0.01	80.35

Table S2

The concentrations of W, Th, or Al, isotopic compositions of W, calculated concentrations of authigenic W and ΔSW-sink, as well as the ages of marine sediments and Fe-Mn crusts. Yang et al. (2022) measured all the isotopic compositions and the concentrations of W in sediments, except for the data of IODP Site U1457, which was obtained from Alam et al. (2022). The ages of sediments from ODP Site 834A and ODP Site 1094 are from Kuwahara et al. (2021) and Hodell et al. (2003). The calculated ΔSW-sink has an ±2 × external standard deviation of ±0.06‰.

Sub-sample ID	**[W] μg/g**	**[Th] μg/g**	**[Al] μg/g**	**$\delta^{186/184}W$ ‰**	**$[W]_{auth}$ μg/g**	**$\delta^{186/184}W_{auth}$‰**	**Age Ma**	**$\delta^{186/184}W_{sw}$ ‰**	**ΔSW-sink ‰**
<u>IODP Site U1366</u>									
D1H1-40	5.63	16.30		0.10	2.68	0.20	2.87	0.54	0.34
D1H2-10	5.80	16.37		0.14	2.84	0.28	7.25	0.55	0.27
D1H2-90	6.03	15.76		0.13	3.18	0.24	10.03	0.57	0.33
D1H2-140	5.37	14.25		0.13	2.79	0.24	11.68	0.58	0.34
D1H3-50	4.58	11.20		0.13	2.55	0.23	13.66	0.60	0.37
D1H3-90	5.53	13.16		0.11	3.15	0.19	14.98	0.60	0.41
D1H4-0	5.58	13.16		0.09	3.20	0.15	16.98	0.60	0.45
D1H4-100	4.19	10.99		0.10	2.20	0.18	20.34	0.58	0.40
D1H4-140	4.03	10.83		0.09	2.07	0.17	21.64	0.58	0.41
D1H5-70	4.00	9.40		0.09	2.30	0.15	24.44	0.58	0.43
D1H5-100	3.88	8.54		0.11	2.33	0.18	25.52	0.58	0.40
D1H5-140	3.61	8.35		0.12	2.10	0.20	27	0.58	0.38
D1H6-0	3.96	8.56		0.07	2.41	0.11	27.4	0.58	0.47
<u>ODP Site 1094</u>									
177-1094-A2H4W(77-78)	0.58	1.49		0.15	0.31	0.27	0.01	0.54	0.27
177-1094-C1H4W(17-19)	0.45	1.30		0.15	0.21	0.30	0.01	0.54	0.24
177-1094-B2H2W(56-58)	0.08	0.14		0.23	0.05	0.33	0.04	0.54	0.21
177-1094-C1H3W(66-70)	0.05	0.09		0.24	0.03	0.35	0.01	0.54	0.19
<u>Fe-Mn crusts</u>									
MDD53-01	42.01	24.74		-0.02	37.53	-0.02	0.00	0.54	0.56
MDD53-02	42.11	28.03		-0.02	37.04	-0.03	5.35	0.54	0.57
CJ01-01	50.52	7.92		-0.05	49.09	-0.05	0.50	0.54	0.59

CJ01-02	59.53	5.91		-0.03	58.46	-0.03	1.50	0.54	0.57
Yaloc-01	77.24	1.21		-0.05	77.02	-0.05	0.00	0.54	0.59
Yaloc-02	79.86	0.36		-0.03	79.79	-0.03	0.00	0.54	0.57
ODP Site 834A									
834A 1H-3W 94-96	0.92	0.31		0.07	0.86	0.07	0.12	0.54	0.47
834A 1H-3W 140-142	0.77	0.36		0.15	0.70	0.16	0.14	0.54	0.38
834A 1H-2W 34-36	0.35	0.26		0.14	0.30	0.16	0.02	0.54	0.38
834A 1H-1W 3-5	0.65	0.22		0.14	0.61	0.15	0.01	0.54	0.39
IODP Site U1457									
3.22	1.55		49500	0.06	0.58	0.14	0.09	0.54	0.40
3.9	1.63		48300	0.09	0.68	0.20	0.11	0.54	0.34
5.17	1.16		36800	0.10	0.44	0.25	0.13	0.54	0.29
5.3	0.97		29600	0.18	0.39	0.43	0.13	0.54	0.11
6.86	1.07		35200	0.10	0.38	0.26	0.15	0.54	0.28
8.36	1.29		46100	0.04	0.38	0.11	0.17	0.54	0.43
9.29	1.38		46500	0.07	0.47	0.19	0.18	0.54	0.35
10.2	1.25		41500	0.11	0.43	0.30	0.19	0.54	0.24
11.1	1.21		39900	0.15	0.43	0.41	0.2	0.54	0.13
13.7	1.37		27700	0.09	0.83	0.14	0.23	0.54	0.40
25.8	1.61		46300	0.11	0.70	0.24	0.43	0.54	0.30
39.8	0.49		17200	0.03	0.15	0.07	0.67	0.54	0.47
57	1.06		33000	0.12	0.41	0.29	0.91	0.54	0.25
80.6	1.64		50300	0.13	0.65	0.31	1.16	0.54	0.23
106.3	2.73		78500	0.11	1.19	0.24	1.31	0.54	0.30
158.9	3.07		59100	0.07	1.91	0.11	1.44	0.54	0.43
171.8	2.98		86400	0.09	1.28	0.20	1.47	0.54	0.34
189.8	3.68		67500	0.13	2.35	0.20	1.52	0.54	0.34
207.3	2.54		70900	0.03	1.15	0.05	1.56	0.54	0.49
245.7	2.59		75100	0.07	1.11	0.15	1.59	0.54	0.39
266.8	2.78		69800	0.06	1.41	0.11	1.59	0.54	0.43
354.2	2.62		73200	0.07	1.18	0.14	1.62	0.54	0.40
368.2	2.70		68800	0.09	1.35	0.17	1.66	0.54	0.37
412.2	2.72		55800	0.13	1.62	0.21	2.33	0.54	0.33
459.3	2.23		58200	0.09	1.09	0.17	2.93	0.54	0.37
500.9	2.22		63500	0.13	0.97	0.28	3.4	0.54	0.26
546.7	2.58		66200	0.10	1.28	0.19	5.63	0.54	0.35
559.3	2.42		71600	0.07	1.01	0.15	5.69	0.54	0.39
577	1.86		61100	0.11	0.66	0.29	5.78	0.54	0.25
702.9	2.27		63200	0.09	1.03	0.19	8.11	0.55	0.36

REFERENCES CITED

Alam, M., Tripti, M., Gurumurthy, G. P., Sohrin, Y., Tsujisaka, M., Singh, A. D., Takano, S., and Verma, K., 2022, Palaeoredox reconstruction in the eastern Arabian Sea since the late Miocene: Insights from trace elements and stable isotopes of molybdenum ($\delta^{98/95}$Mo) and tungsten ($\delta^{186/184}$W) at IODP Site U1457 of Laxmi Basin: Palaeogeography, Palaeoclimatology, Palaeoecology, v. 587, p. 110790.

Hodell, D. A., Charles, C. D., Curtis, J. H., Mortyn, P. G., Ninnemann, U. S., and Venz, K. A., 2003, (Table T7) Stable oxygen and carbon isotope ratios of Neogloboquadrina pachyderma (sinistral) at ODP Site 177-1094 in the Southern Ocean, In supplement to: Hodell, DA et al. (2003): Data Report: Oxygen isotope stratigraphy of ODP Leg 117 sites 1088, 1089, 1090, 1093, and 1094. In: Gersonde, R; Hodell, DA; Blum, P (eds.) Proceedings of the Ocean Drilling Program, Scientific Results, College Station, TX (Ocean Drilling Program), 177, 1-26, https://doi.org/10.2973/odp.proc.sr.177.120.2003, PANGAEA.

Kuwahara, Y., Yasukawa, K., Fujinaga, K., Nozaki, T., Ohta, J., Sato, H., Kimura, J. I., Nakamura, K., Yokoyama, Y., and Kato, Y., 2021, Rapid coupling between solid earth and ice volume during the Quaternary: Sci Rep, v. 11, no. 1, p. 5695.

Ling, H.-F., Jiang, S.-Y., Frank, M., Zhou, H.-Y., Zhou, F., Lu, Z.-L., Chen, X.-M., Jiang, Y.-H., and Ge, C.-D., 2005, Differing controls over the Cenozoic Pb and Nd isotope evolution of deepwater in the central North Pacific Ocean: Earth and Planetary Science Letters, v. 232, no. 3, p. 345-361.

Liu, J., Qu, Y., Li, W., Wei, G., Sun, Q., Ling, H., and Chen, T., 2022, in Chinese, Elemental distribution pattern and forming mechanism of the two types of phosphates in ferromanganese crust in Western Pacific Ocean and their implications: Marine Geology & Quaternary Geology, v. 42, no. 2, p. 36-45.

Rudge, J. F., Reynolds, B. C., and Bourdon, B., 2009, The double spike toolbox: Chemical Geology, v. 265, no. 3-4, p. 420-431.

Rudnick, R. L., and Gao, S., 2014, 4.1 - Composition of the Continental Crust, *in* Holland, H. D., and Turekian, K. K., eds., Treatise on Geochemistry (Second Edition): Oxford, Elsevier, p. 1-51.

Stubbs, D., Yang, R., Coath, C. D., John, T., and Elliott, T., 2022, Tungsten isotopic fractionation at the Mariana arc and constraints on the redox conditions of subduction zone fluids: Geochimica et Cosmochimica Acta, v. 334, p. 135-154.

van de Flierdt, T., Frank, M., Halliday, A. N., Hein, J. R., Hattendorf, B., Günther, D., and Kubik, P. W., 2004, Tracing the history of submarine hydrothermal inputs and the significance of hydrothermal hafnium for the seawater budget—a combined Pb–Hf–Nd isotope approach: Earth and Planetary Science Letters, v. 222, no. 1, p. 259-273.

Yang, R., Li, T., Stubbs, D., Chen, T., Liu, S., Kemp, D. B., Li, W., Yang, S., Chen, J., Elliott, T., Dellwig, O., Chen, J., and Li, G., 2022, Stable tungsten isotope systematics on the Earth's surface: Geochimica et Cosmochimica Acta, v. 322, p. 227-243.

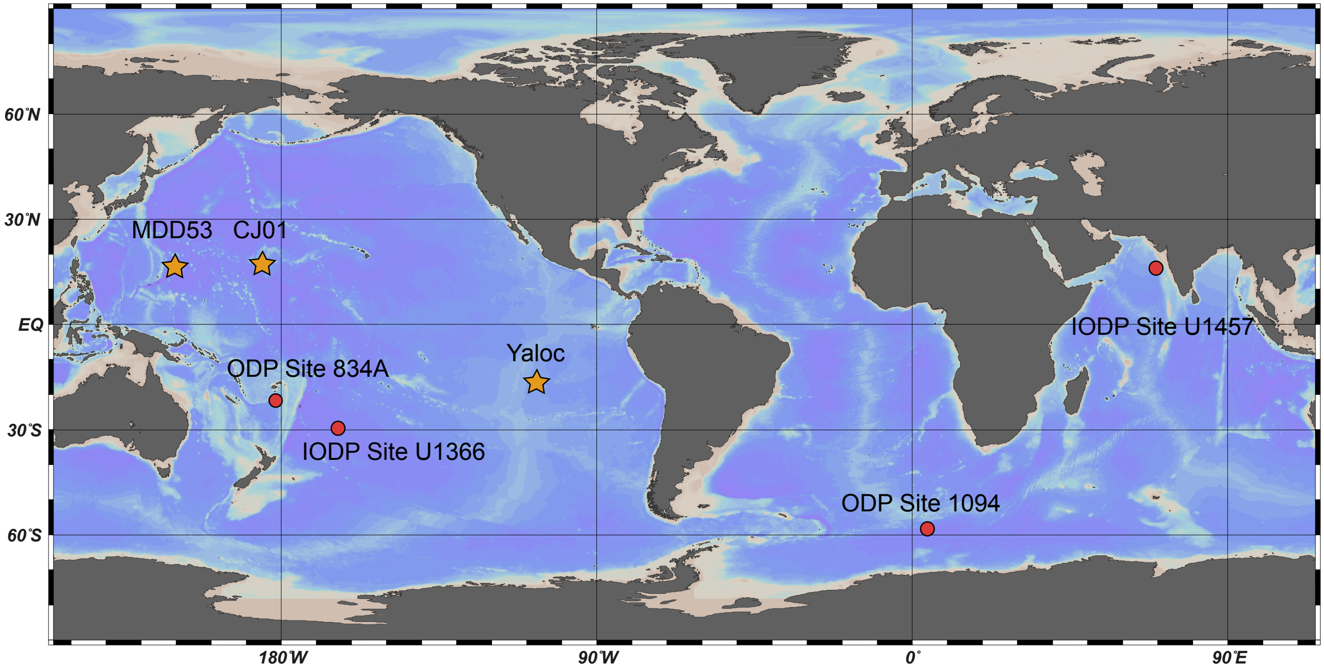

60°N
30°N
EQ
30°S
60°S
180°W
90°W
0°
90°E
MDD53
CJ01
Yaloc
ODP Site 834A
IODP Site U1366
IODP Site U1457
ODP Site 1094

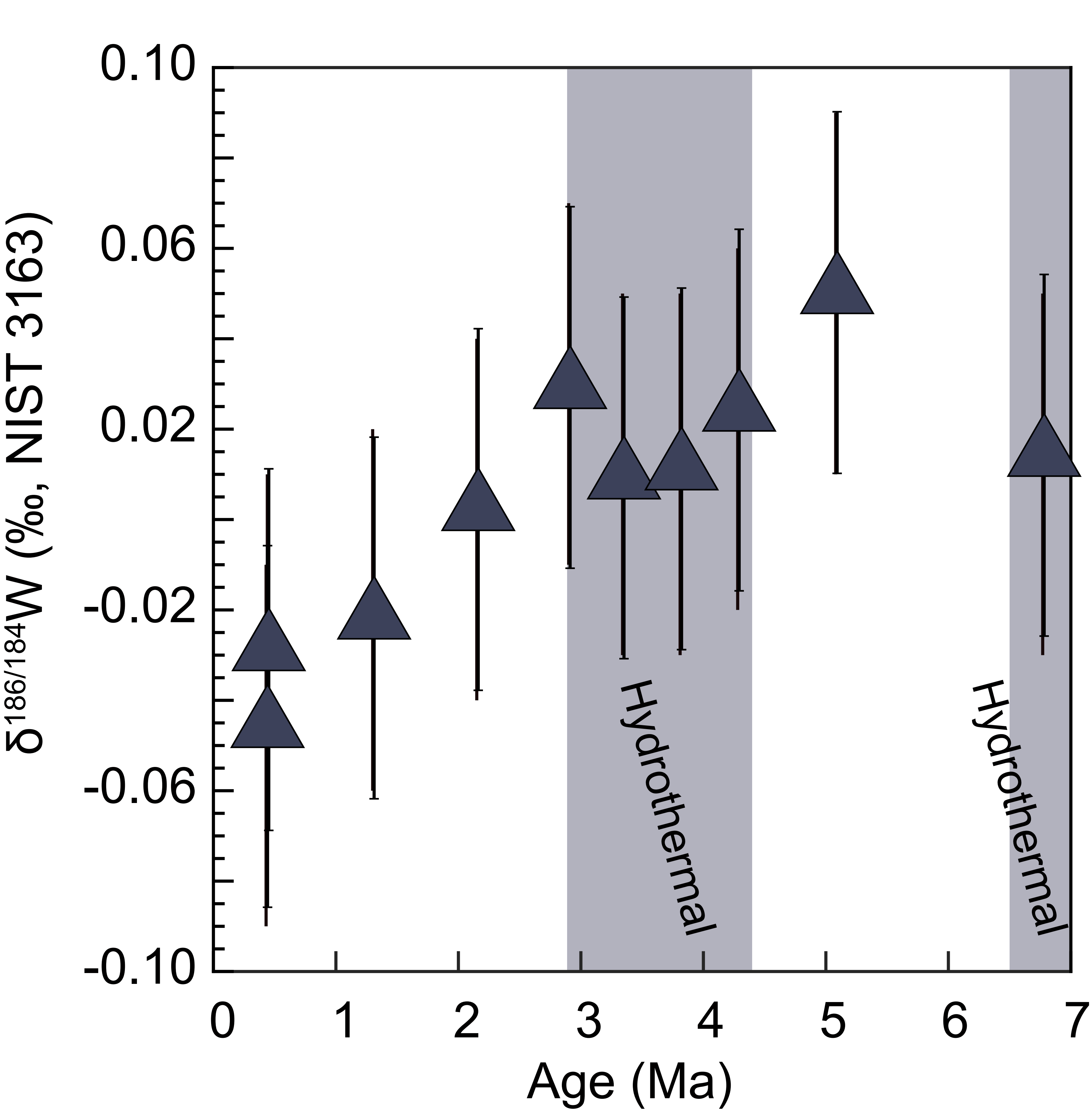

0.10
0.06
0.02
-0.02
-0.06
-0.10
δ186/184W (‰, NIST 3163)
0
1
2
3
4
5
6
7
Age (Ma)
Hydrothermal
Hydrothermal

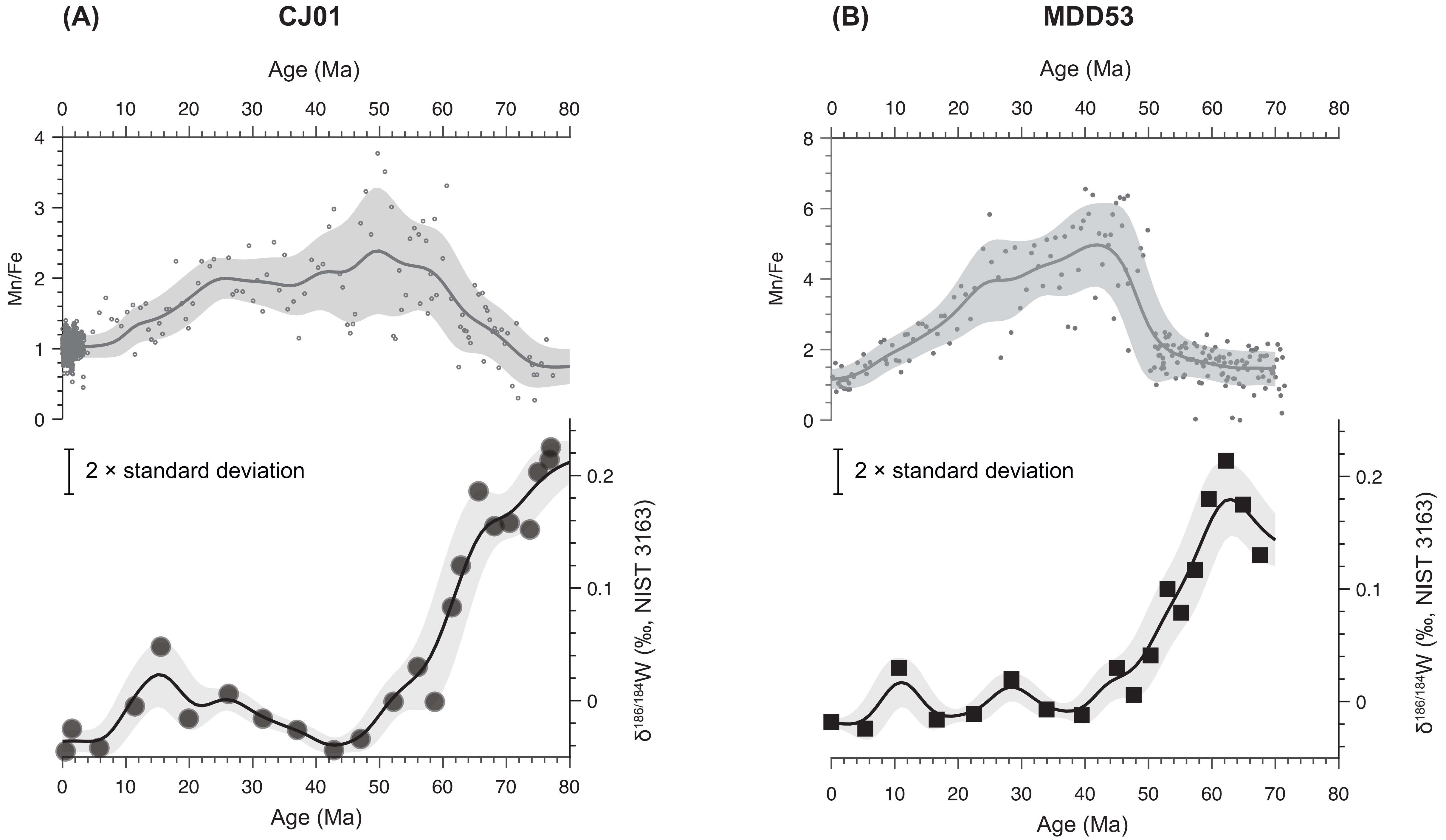
(A)
CJ01
(B)
MDD53
Age (Ma)
Mn/Fe
2 × standard deviation
δ186/184W (‰, NIST 3163)
Age (Ma)

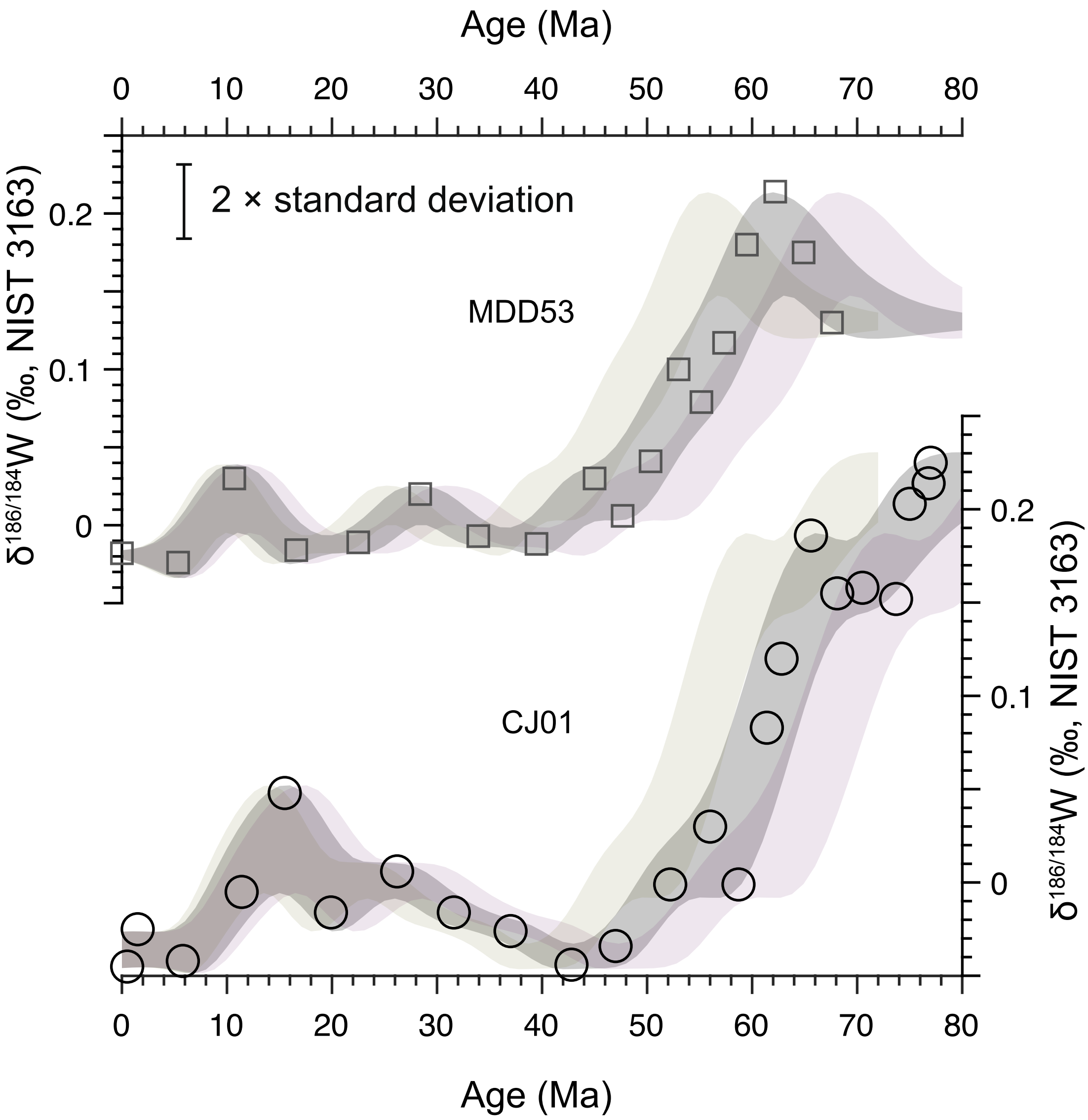

Age (Ma)
0
10
20
30
40
50
60
70
80
2 × standard deviation
MDD53
CJ01
δ186/184W (‰, NIST 3163)
0.2
0.1
0
Age (Ma)